Chapter 3

Polyindole functionalized g-C_3N_4 nanosheets via in-situ chemical polymerization for its improved electrochemical performance

This chapter deals with a brief description on modification of graphitic C_3N_4 by polyindole (PIn) in order to enhance the electrochemical phenomenon. It also discribes a feasible synthesis method in this context along with various characterization techniques to study the structural, morphological and electrochemical properties.

3.1 Introduction

As an energy storage device, the electrochemical capacitor has been considered with immense interest worldwide to solve the energy crisis and prevent the uncontrolled consumption of fossil fuels. This is due to high power density, energy density, fast charge-discharge rate, better cycle life, and excellent reversibility [Zhau et al. (2011), Xiao et al. (2013), Wang et al. (2016), Blomquist et al. (2016)]. The functional mechanism of charge storage/accumulation in supercapacitors could explain under two classes. The first one is called an electric double-layer capacitor (EDLC), where the formation of the double layer caused by charge separation between the electrode and the electrolyte. However, in the second class that is called pseudocapacitoror faradaic supercapacitors, the charge storage takes place as a result of redox reaction or faradaic reaction [Wang et al. (2016)]. For a real application, intensive research has been carried out to develop new capacitive electrode materials with significant improvement in its charge storage capacity. In this regard, various carbon-based nanomaterials [Huang et al (2015), Wang et al. (2018)], conducting polymers [Ghosh et al. (2016), Fong et al. (2017)], and transition metal oxides/ hydroxides [Shi et al. (2014), Zhang et al. (2017), Sharma et al. (2018)] are reported for supercapacitor/pseudocapacitor application. Due to eco-friendly, low cost, and semiconducting nature of carbon-based nanomaterials, the earlier research work shows diversified interests and particularly such materials are frequently used as electrode materials though has poor electrochemical performance due to interfacial defects as well as less conducting path that prevents the charge transfer on the surface as well as inside the electrode materials. In order to short out such issues, researchers have integrated some conducting parts like incorporation of

conducting additives, doping, architectural orientations etc. with carbon or carbon based nanomaterials [Lu et al. (2019), Zhou et al. (2018)]. For example, surface modification and doping, is a highly effective way to organize the surface textures and nanostructures of desired materials in order to improve their electrochemical performance. In other words, surface-modified nanostructured carbon provides a better path/network for interstitial connections through which charge can move rapidly [Subramaniyam et al. (2017)]. On the other hand, the presence of redox-center at the electrode materials' surface leads to faradaic reactions and manifested the pseudocapacitance. Hence, the overall increment in the electrochemical specific capacitance is directly related to the interfacial contact, the interface of the material's, morphology, composition, and surface area. Among many known analogs of carbon nanostructures, g-C_3N_4 having 2D sheets of tri-s-triazine connected via tertiary amines like structures with its high surface area (2500 m^2g^{-1}) and bandgap of ~2.7eV. Therefore extensive research is going on in the recent past as a metal-free semiconductor for visible-light photocatalysis and electrocatalysis [Liu et al. (2011), Gao et al. (2019), Yanget al. (2013), Chang et al. (2013), Li et al. (2019)]. Due to strong van der Waals forces between g-C_3N_4 layers, they quickly get restacked, and cause of poor conductivity or electron mobility and hence rarely employed as energy storage material [Tahir et al. (2013), Tahir et al. (2014), Luo et al. (2019)]. However, the presence of high N content along with π-conjugated systems within a g-C_3N_4 layer, which is an advantageous parameter for better electrode-electrolyte wettability and surface polarity. Furthermore, due to N-heteroatom, it has an additional electron donor/acceptor ability-based more reaction sites for improved pseudocapacitive

behavior [Tahir et al. (2014)]. Such kind of ability may be beneficial for synergistic contact between g-C_3N_4 layer and another component not only to provide stable hybrids but also enhancing their interfacial contact and microstructure, which is directly related to the electrochemical performance of nanohybrids [Luo et al. (2019)]. In order to achieve such interfacial hybrids, various combinations like metal oxides/ hydroxides, sulfides, and graphene with g-C_3N_4 as a binary/ tertiary hybrids are reported for electrochemical applications [Shi et al. (2015), Zhanget al. (2015), Ye et al. (2016), Wu et al. (2017), Guo et al. (2017), Zhao et al. (2017), Jiang et al. (2017), Dong et al. (2017), Zhang et al. (2017), Ansari et al. (2017), Lin et al. (2017), Vattikuti et al. (2018), Wei et al. (2018), Xu et al. (2019)].

Conducting polymers (CPs) are other fantastic candidates for energy devices and supercapacitors due to their high conductivity, flexibility, low cost, easy processability, and intercalation/ de-intercalation ability of ions of electrolyte [Meng et al. (2017)]. Various kinds of CPs like polyaniline (PAni), polyindole (PIn), polypyrrole (PPY), polythiophene (PTh) and their derivatives are well studied and reported [Verma et al. (2020), Jiang et al. (2019), Ren et al. (2016), Sun et al. (2014)].

Among the various studied CPs as a surface modifier, PIn is an excellent electroactive material, having aforementioned outstanding advantages like low production cost, high stability, good conductivity, non-toxicity, and fast electrochemical response [Dubey et al. (2015), Raj et al. (2015), Zhou et al. (2016), Verma et al. (2018)]. However, there are few reports are available for g-C_3N_4-CP based nanohybrids as metal-free pseudo-capacitive electrode material. For example, Chen et al.(2015) prepared PEDOT/g-C_3N_4 binary electrode material for supercapacitor applications with Cs value 137 Fg^{-1} in

H_2SO_4 and 200 Fg^{-1} in Na_2SO_4 at a current density of 2.0 Ag^{-1}. Shayeh et al. (2018) reported Cs value of 175 Fg^{-1} at 16 Ag^{-1} current density for polyaniline coated reduced graphene oxide/g-C_3N_4/Ag_2O composite. However, to the best of our knowledge, controlled modification of g-C_3N_4 with PIn as a metal-free electrode material is not reported yet in the literature for electrochemical applications.

Herein this chapter, we are reporting the controlled surface modification of g-C_3N_4 using a simple and one-step *in-situ* chemical polymerization of indole monomer to obtain g-C_3N_4-PIn nanohybrids. A varied amount of indole monomer controls the microstructure and interfacial interactions at g-C_3N_4 nanoflakes during polymerization. Furthermore, electrochemical studies of the as-synthesized nanohybrids along with parental counterparts are performed without using any binder and conductive carbon in relevance to improved electrochemical performance. We observed that 1:2 g-C_3N_4-PIn nanohybrid electrode exhibits better electrochemical performance compared to other nanohybrids (1:0.5 and 1:5 g-C_3N_4-PIn nanohybrids) as well as bare g-C_3N_4 and pure PIn.

3.2. **Materials and methods**

3.2.1. Materials

Urea, ammonium peroxodisulfate (APS) and hydrochloric acid were obtained from Fisher Scientific, India. Indole (≥99%) was procured from Aldrich, USA. Milli Q water with resistivity 18.2 MΩ cm was used throughout all experiments.

3.2.2. Synthesis of g-C_3N_4

The bulk g-C_3N_4 was prepared by using urea as a nitrogen-rich cheap precursor, according to the previous literature [Liu et al. (2011)]. In a feasible synthetic protocol,

urea (10.0 g) was grounded in mortar-pestle and placed in a covered alumina crucible and heated up to 550°C at a heating rate of 4°C/minute in a muffle furnace for 4 h under ambient condition. After natural cooling to room temperature, the pale yellow product was collected and washed several times with water and ethanol, respectively. Finally, the material was dried in a vacuum oven overnight at 60°C and stored for further use.

3.2.3. Synthesis of g-C_3N_4-PIn Nanohybrids

g-C_3N_4-PIn nanohybrids were synthesized with varying weight ratio as 1:0.5, 1:2 and 1:5 by using our earlier synthetic protocol for in-situ chemical polymerization, where the molar ratio of monomer and the oxidizing agent is 1:2 [Dubey et al. (2015)]. In order to prepare 1:0.5 g-C_3N_4-PIn nanohybrid, 10 mg of g-C_3N_4 flakes was ultrasonicated in 20 mL water for 1 h to get homogeneous and stable dispersion of g-C_3N_4 nanoflakes. After that, 5.0 mg indole monomer was dissolved in 500μL ethanol solution and added dropwise into the above aqueous dispersion of g-C_3N_4 under vigorous stirring and further ultrasonicated for another 20 min at room temperature. The reaction mixture was stirred for another 30 min for effective adsorption of monomer over the surface and inside the stacked g-C_3N_4 nanoflakes. A freshly prepared 10 mL aqueous APS (1.0M) solution as an oxidizing agent was dropped into the above mixture under constant magnetic stirring in order to start polymerization of indole. Finally, 500 μL of 12.0M HCl was also added to facilitate *in-situ* polymerization. After 30 minutes, the reaction mixture was kept overnight in dark at 25°C without any disturbance for complete polymerization. Similarly, other variants of g-C_3N_4-PIn nanohybrids (*i.e.* 1:2 and 1:5) were also synthesized using 20 and 50 mg

indole monomer, respectively *via* same process with a fixed amount of g-C_3N_4 (10 mg) for each. The greenish solid residue obtained after 24 h was collected by centrifugation and washed several times with water followed by ethanol to remove unconsumed monomer and other side-products. The obtained nanohybrids were dried overnight in a vacuum oven at 60°C and stored for further use. Pure PIn was also synthesized using same protocol for comparison.

3.2.4. Electrode modification

To perform electrochemical studies, the modification of glassy carbon electrode (GCE; of diameter 3.0 mm) was done as follows: GCE was polished with 0.3 μm alumina slurry before every use followed by ultrasonic cleaning with water & absolute ethanol, and finally dried under vacuum. The electrode modification was performed by drop casting method in which 10 μL dispersion (5 mg/mL in ethanol) of desired materialis drop coated onto the polished GCE surfaceand dried in vacuum. (*Note*: The dispersion of desired material is prepared without using any binder or conductive carbon)

3.2.5.Chemical structure of PIn

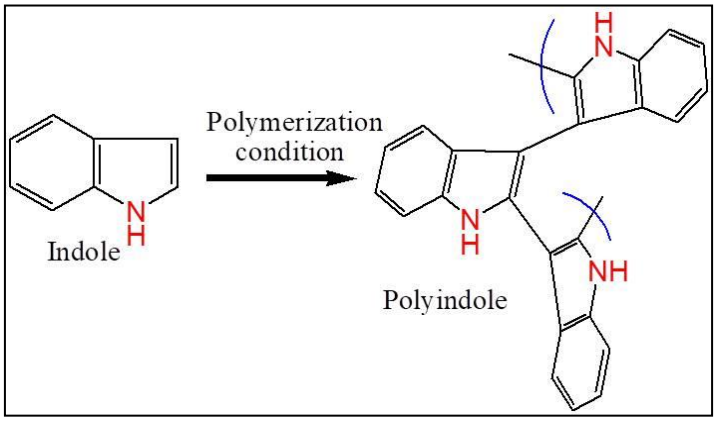

Figure 3.1 Schematic presentation of PIn structure

A well known accepted chemical structure of PIn is shown in figure 3.1. Herein, the point of fusion of polymer chains are C2- and C3-position of indole monomers. Our adopted *in-situ* polymerization procedure is the consequence of such kind of fusion which is justified experimentally by number of researchers [Tiwari et al. (2015)].

3.3. **Results and Discussion**

3.3.1. Structural Studies

XRD analysis:

Combined XRD patterns of bare g-C_3N_4, g-C_3N_4-PIn nanohybrids, and pure PIn are presented in Figure 3.2. The XRD pattern of bare g-C_3N_4 (Figure 3.2a) has two characteristic peaks at 2θ value ~27° and ~13° corresponding to the (002) and (100) diffraction planes, respectively [Liu et al. (2011)]. The first peak is attributed to the interlayer stacking of the conjugated aromatic system and the second one is responsible for the in-planar repeating unit of tri-s-triazine moiety present in the g-C_3N_4 [Liu et al. (2011), Yang et al. (2013), Chang et al. (2013)]. Pure PIn (see Figure 3.2e) has a characteristic feature of the broad amorphous band centered between 15 to 30° [Verma et al. (2018)]. After the surface modification of g-C_3N_4 with PIn (*cf.* Figure 3.2 b, c, d), we observed significant broadening in (002) plane peak along with slight suppression of (100) plane peak intensity corresponding to the g-C_3N_4 and disappearance of the broadband feature of pure PIn. This kind of things are attributed due to alteration of conjugation and stacking pattern within g-C_3N_4 and reveals the successful formation of g-C_3N_4-PIn nanohybrids along with interfacial interaction between them [Chen et al. (2015)]. For 1:2 g-C_3N_4-PIn nanohybrid, the above

modification in the XRD pattern is quite significant and suggests good surface adhesion at such a combination of counterparts.

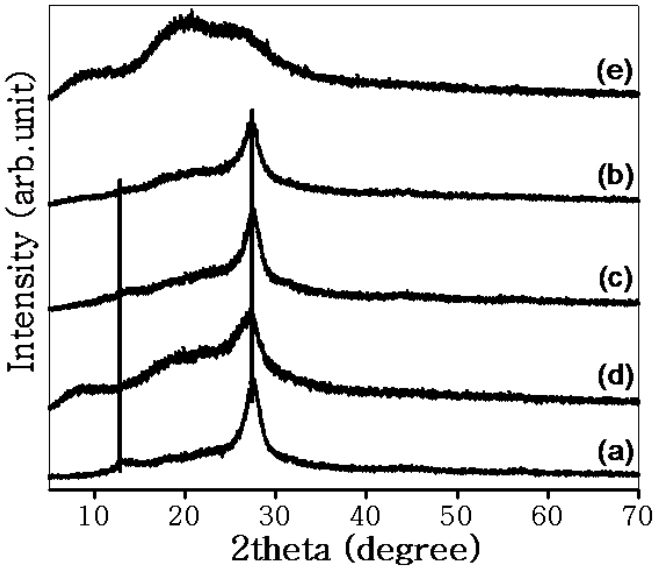

Figure 3.2 XRD pattern of (a) bare g-C_3N_4, (b) 1:0.5, (c) 1:2, (d) 1:5 g-C_3N_4-PIn nanohybrids and (e) pure PIn.

UV–Vis spectra:

UV–Vis spectra of the as-synthesized materials are recorded in ethanol and displayed in Figure 3.3. We have observed effective absorbance below 450 nm along with a major peak at ~321 nm for bare g-C_3N_4 (see Figure 3.3a) which corresponds to the electronic transitions from the valance band to the conduction band [Liu et al. (2011), Tahiret al. (2014), Ye et al. (2016)]. Pure PIn shows the characteristic peaks at around 290, 304, 348, 374, 392, and 524 nm (see Figure 3.3d) which are due to the π-π*, n-π* transitions, and overlapping bands of PIn polaronic excitations [Dubey et al. (2015), Verma et al. (2018), Tiwari et al. (2015)]. For 1:0.5 g-C_3N_4-PIn nanohybrid (*see* Figure 3.3b), a minor signature of PIn along with the predominant feature of g-C_3N_4 and a slight shift in the peak position was observed. However, for 1:2 g-C_3N_4-PIn

nanohybrid (*see* Figure 3.3c), we can significantly observe the absorbance peaks corresponding to the PIn.

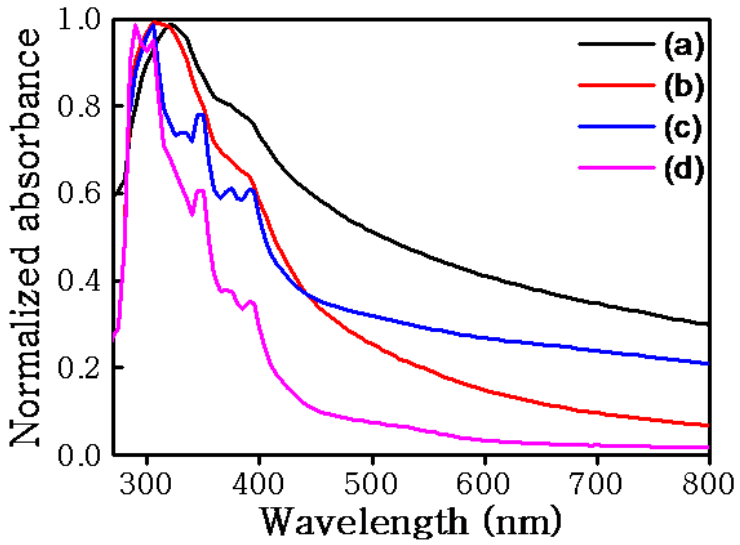

Figure 3.3 Combined UV-Vis spectra of (a) bare g-C_3N_4, (b) 1:0.5, (c) 1:2 g-C_3N_4-PIn nanohybrids and (d) pure PIn in ethanol.

On comparing the absorbance spectra of nanohybrids, the major peak responsible for the bare g-C_3N_4 at 321 nm was blue-shifted to 305 nm in the case of 1:2 g-C_3N_4-PIn nanohybrid and there was a sharp feature of the peak, which is consistent with the pure PIn. This is attributed due to the good interfacial interaction resulting in synergistic contact between polymer and g-C_3N_4 at this composition.

ATR and Raman analysis:

The changes in chemical structures of the as-synthesized nanohybrids are further confirmed by ATR as well as Raman analysis and presented in Figure 3.4 and Figure 3.5, respectively. The ATR spectrum of bare g-C_3N_4 (Figure 3.4a) shows the characteristic band at around 1406, 1456, 1566, and 1639 cm^{-1}, which are due to the typical stretching vibrations of repeating units derived from heptazine moiety of g-

C_3N_4 [Liu et al. (2011), Yang et al. (2013)]. The bands corresponding to the 1321 and 1236 cm^{-1} are due to the stretching vibrations of C-N(-C)-C or C-NH-C connected units within g-C_3N_4 [Liu et al. (2011)]. Furthermore, a sharp peak at ~812 cm^{-1} is responsible for the out-of-plane bending mode deformation of tri-s-triazine moiety and heptazine rings [Liu et al. (2011), Chen et al. (2015)]. For pure PIn (Figure 3.4e), a broad peak nearly 3300 cm^{-1} (N-H stretching mode) along with vibrational peak around 1568 cm^{-1} (N-H deformation mode) are observed which confirms that N-site of PIn chain is free and not involved in polymerization [Tiwari et al. (2015)]. Some characteristic vibrations in the 1100-1600 cm^{-1} frequency range are due to the carbon skeleton with single and double bonds in the benzene rings [Tiwari et al. (2015)]. A sharp vibrational peak at ~742 cm^{-1} in the case of pure PIn sample is the signature of the out-of-plane deformation of the C-H bond in the benzene ring and establishes that benzene ring is also not participating in polymerization process [Verma et al. (2018), Tiwari et al. (2015)]. The ATR of g-C_3N_4-PIn nanohybrids (as shown in Figure 3.4b, c, d) are clearly displayed the most of the characteristic peaks of g-C_3N_4 retained with overlapping by PIn. The intensity of ~742 cm^{-1} peak is changed according to the polymer amount which becomes more intense as the polymer amount increases successively (black drop line at 742 cm^{-1} region in Figure 3.4). Furthermore, the intensity of ~812 cm^{-1} peak reduces gradually with a slight shift at a lower value (black drop line at ~812 cm^{-1} in Figure 3.4) by increasing the mass ratio of PIn. These deviations indicate that there is some overlapping/ interaction between g-C_3N_4 and PIn, which again confirms the successful surface coating of g-C_3N_4 nanoflakes. For 1:2 g-C_3N_4-PIn nanohybrid (*see* Figure 3.4c), the above two peaks, which are at ~805

cm^{-1} (due to g-C_3N_4) and 741 cm^{-1} (due to PIn), appear of the nearly same intensity, which indicates better surface interaction/ coating at this particular composition. Raman spectra of bare g-C_3N_4, pure PIn, and 1:2 g-C_3N_4-PIn nanohybrid are presented in Figure 3.5. In the Raman spectra of bare g-C_3N_4 (*see* Figure 3.5a), broadband in between ~1000-1600 cm^{-1} was observed, which is consistent with the reported value in the literature [Jiang et al. (2016)]. For pure PIn (*see* Figure 3.5b), the peaks at ~ 1614 and 1579 cm^{-1} are due to the asymmetric and symmetric stretching of the aromatic structure of PIn. The peaks around 1386 and 1329 cm^{-1} are originated due to the benzoic ring stretching. The peaks at ~1241 and 1157 cm^{-1} are due to the out-of-plane and in-plane deformation of N-H moiety, while the peak at ~ 1152 cm^{-1} is due to the out of plane deformation of C-H bond [Raj et al. (2015)].

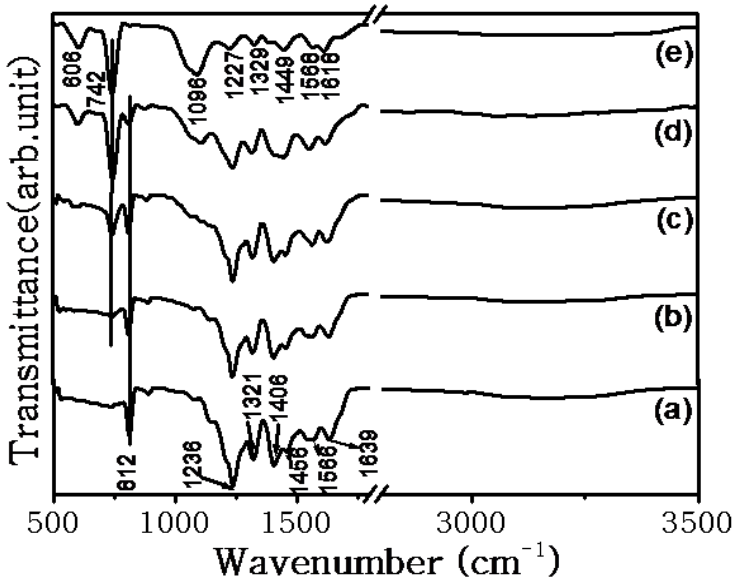

Figure 3.4 ATR spectra of (a) bare g-C_3N_4, (b) 1:0.5, (c) 1:2, (d) 1:5 g-C_3N_4-PIn nanohybrids and (e) pure PIn.

Furthermore, the Raman spectrum of the 1:2 g-C_3N_4-PIn nanohybrid (*see* Figure 3.5c) shows a predominant characteristic of PIn and disappearance/overlap of the broadband

feature of g-C_3N_4 (inset of Figure 3.5c enlarged view of Raman spectra of PIn and g-C_3N_4-PIn nanohybrid), which signifies good coating of PIn over g-C_3N_4 nanoflakes and support our microscopic and other spectroscopic studies. Apart from all the signature peaks of PIn present in this nanohybrid, we surprisingly observed one new peak at ~570 cm^{-1}, which may be attributed to the significant interfacial interaction between two counterparts and formation of a new interfacial bond which appears after polymerization, resulting some in/out of plane deformation [Raj et al. (2015), Chen et al. (2015)].

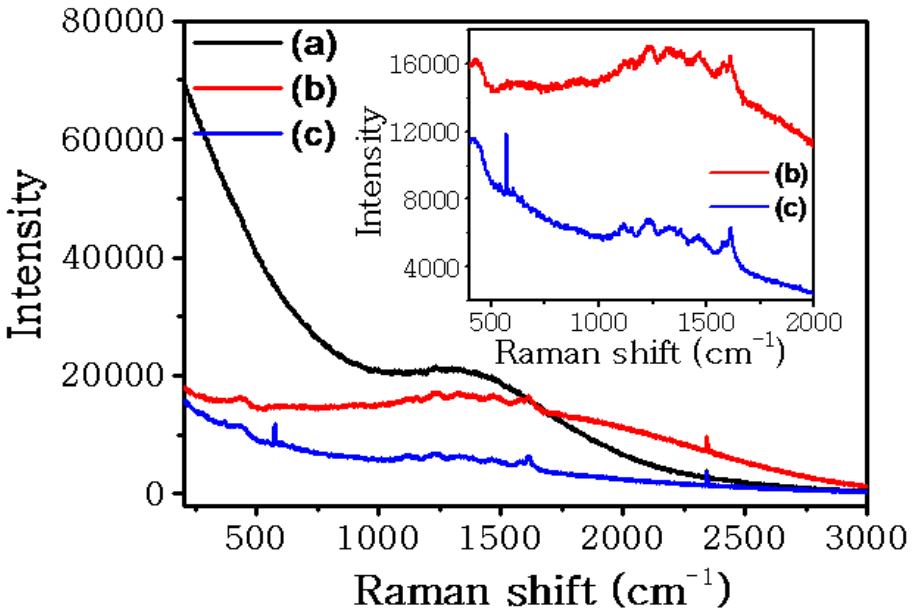

Figure 3.5 Raman spectra of (a) bare g-C_3N_4, (b) pure PIn and (c) 1:2 g-C_3N_4-PIn nanohybrid.

XPS analysis:

XPS was performed to evaluate the surface chemical components and chemical state of the as-prepared materials presented in Figure 3.6. The survey spectrum of g-C_3N_4 (Figure 3.6A) and 1:2 g-C_3N_4-PIn nanohybrids (Figure 3.6B) shows three peaks

corresponds to C1s, N1s, and O1s elements [Greczynski et al. (2020)]. After the g-C_3N_4 surface modification via PIn, it is observed that the relative intensity corresponding to C1s, N1s and O1s has changed (*cf.* Figure 3.6A and Figure 3.6B). The 1:2 g-C_3N_4-PIn nanohybrids have less N content however O content becomes high because of PIn have low ratio C/N elements. For more details, we deconvolute the N1s and C1s peak separately (shown in Figure 3.6C-E). The g-C_3N_4 has four peaks indicating four types N at 398.48 eV for (C=N–C of triazine rings), 399.73 eV for (N–$(C)_3$ tertiary nitrogen), 401.22 eV for (C–N–H of amino groups) and 404.22 eV for N-Oxide (*see* in Figure 3.6C) [Tejasvi et al. (2020), Gao et al. (2019)]. In the case of the 1:2 g-C_3N_4-PIn nanohybrids (*see* in Figure 3.6D), only two peaks are located at 399.81 eV and 401.74 eV which is due to C-N and pyrrolic N-H group and typical indicating of PIn existence [Chulliyote et al. (2017)]. The presence of pyrrolic nitrogen may influence the electrochemical properties of synthesized nanohybrids. These observations validate the surface of g-C_3N_4 is well covered with PIn, which agrees well with the SAED (discussed later). The C1s peaks for g-C_3N_4 and 1:2g-C_3N_4-PIn nanohybrids (as in Figure 3.6E(a-b)), in which the peak located at 287.89 eV and 284.46 eV corresponding to (N–$(C)_3$ and C–C respectively (Figure. 3.6 Ea for g-C_3N_4). After surface modification, there is a visible change appeared (*cf.* Figure 3.6Ea and b) The peak at 287.89 eV corresponding to (N–$(C)_3$is vanished, however another peak at 284.66 eV with an additional peak near 286 eV which can be assigned to a typically C-C and C=N functionality related to the PIn. These results attributed to the dominancy of PIn which is to cover the g-C_3N_4 surface homogenously.

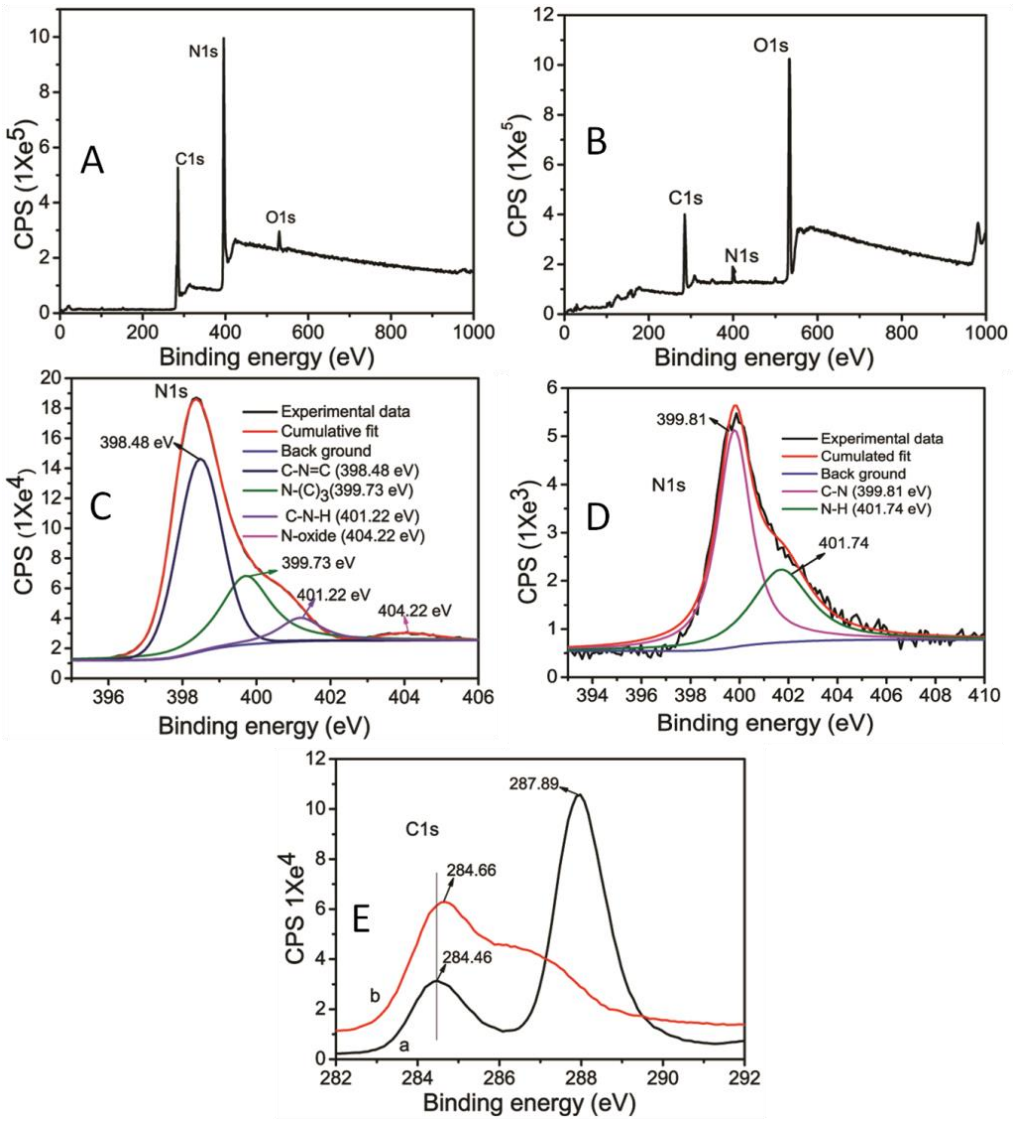

Figure 3.6 XPS spectra of (A) bare g-C_3N_4, (B) 1:2, g-C_3N_4-PIn nanohybrids full survey, (C) and (D) deconvolute peak of N1s and (E) C1s peaks for g-C_3N_4 and 1:2g-C_3N_4-PIn nanohybrids, respectively.

3.3.2 Morphological analysis

The morphological features of bare g-C_3N_4, pure PIn, and as-synthesized g-C_3N_4-PIn nanohybrids were characterized by HRSEM (Figure 3.7) and TEM (Figure 3.8) analysis. The bare g-C_3N_4 (Figure 3.7a) displays lamellar flake-like structure and multilayer aggregation [Chang et al. (2013), Wu et al. (2017), Chen et al. (2015)].

After coating with PIn (Figure 3.7b, c, d), the g-C_3N_4-PIn nanohybrids surface morphology changed significantly (*see* Figure 3.7b-d). A 1:2 g-C_3N_4-PIn nanohybrid (Figure 3.7c) exhibits a network-like structure and a good coating of PIn resulting smooth surface feature compared to other g-C_3N_4-PIn nanohybrids *(cf.* Figure 3.7b and 3.7d). The formation of a uniform layer of PIn over g-C_3N_4 is attributed to good interaction between the g-C_3N_4 and PIn interface. However, less as well as a high amount of PIn result non-uniform layer over the g-C_3N_4 surface. The 1:0.5 g-C_3N_4-PIn is showing g-C_3N_4 characteristics and 1:5 g-C_3N_4-PIn shows PIn characteristics dominantly. Because of the strong π-π interaction between the g-C_3N_4 sheets and the PIn chain, which results in agglomerations in its pristine form which are reflected in their poor electrochemical performance (discussed later). Thus herein, the 1:2 g-C_3N_4-PIn has a proper amount of PIn to cover the g-C_3N_4 surface homogenously and reduces path length and resistance. Consequently, such surface modification can facilitate fast charge transportation in between electrode and electrolyte [Chen et al. (2015), Shayeh et al. (2018)]. For elemental information, EDX for g-C_3N_4 and 1:2 g-C_3N_4-PIn nanohybrid (shown in Figure 3.7a' and b' respectively) have performed. This spectrum shows the presence of only N and C, which are the desired elements. Also, there is Gold (Au) and Aluminum (Al) peak, because of Al stub used followed by gold coating. The closed overview of the microstructures of bare g-C_3N_4, g-C_3N_4-PIn nanohybrids, and pure PIn are observed by TEM (illustrated in Figure 3.8) with selected area diffraction pattern (SAED). It was observed that the PIn is smoothly covered the surface of g-C_3N_4 and form a close interface between them, which is consistent with our HRSEM observations. SAED pattern of g-C_3N_4, 1:2 g-C_3N_4-PIn

nanohybrids and PIn are represented (as Figure 3.8f-h). The SAED of g-C_3N_4 (*see* Figure 3.8f) is showing two rings corresponding to XRD peak ~13° (100) and at ~27° (002) planes and suggesting for semi-crystalline nature of g-C_3N_4. The 1:2 g-C_3N_4-PIn (Figure 3.8g) gives a diffuse pattern due to the amorphous nature of PIn is suggesting a complete surface modification of g-C_3N_4 via PIn. SAED of pure PIn (Figure 3.8h) has a diffuse pattern due to amorphous nature.

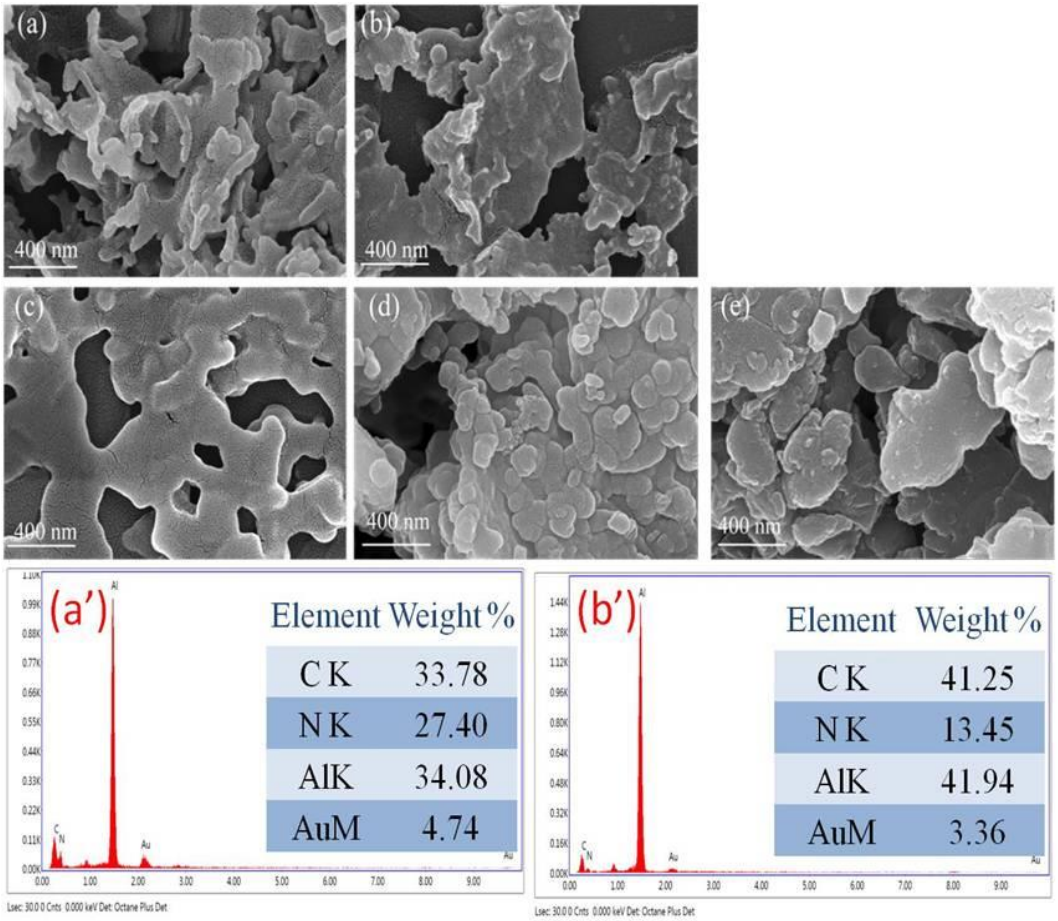

Figure 3.7 SEM image of (a) bare g-C_3N_4, (b) 1:0.5, (c) 1:2, (d) 1:5 g-C_3N_4-PIn nanohybrids, (e) pure PIn and EDX of (a') g-C3N4 and (b') 1:2 g-C_3N_4-PIn nanohybrids

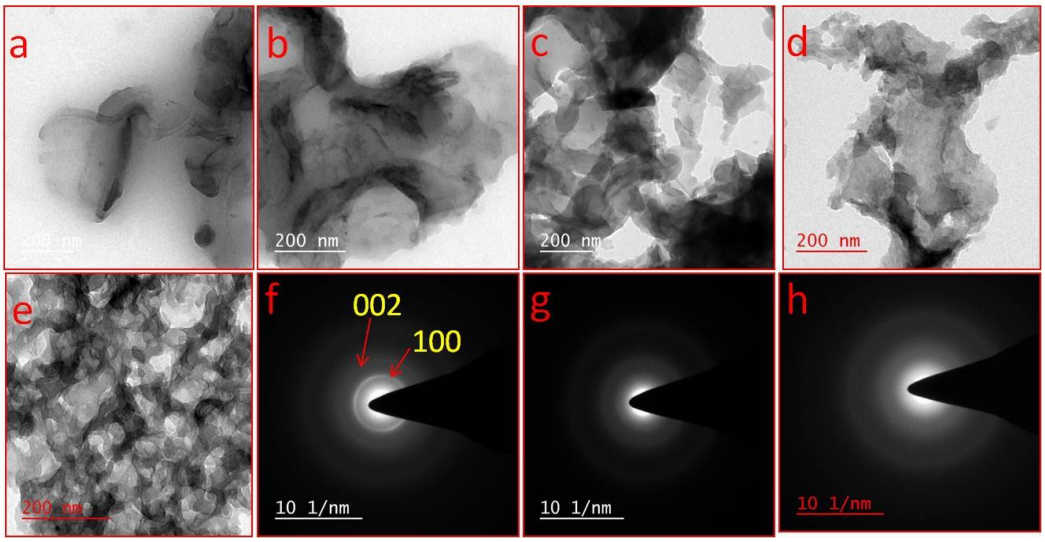

Figure 3.8 TEM image of (a) bare g-C_3N_4, (b) 1:0.5, (c) 1:2, (d) 1:5 g-C_3N_4-PIn nanohybrids, (e) pure PIn and (f) SAED pattern of g-C_3N_4, (g) 1:2 g-C_3N_4-PIn nanohybrids, (h) pure PIn

3.3.3 Thermal analysis:

Furthermore, to establish the effect of PIn coating on the g-C_3N_4 surface, thermal stability studies were also performed *via* TGA which depicted in Figure 3.9. The experimental observation reveals the significant vibrant behavior of the degradation process. The weight loss in the TGA curve of bare g-C_3N_4, pure PIn, and 1:2 g-C_3N_4-PIn nanohybrid below 200 °C were assigned due to the removal of physically adsorbed and intercalated water (*see* Figure 3.9a-c) [Shi et al. (2015)]. The second weight loss after 500 °C of bare g-C_3N_4 (Figure 3.9a) occurs due to the dissociation of the C-N bond and thermal breakdown of the constructing fragments [Shi et al. (2015), Zhang et al. (2017)]. The pure PIn (Figure 3.9b) shows weight loss in between 200 to 300 °C, which corresponds to the removal of polymer π bonding and their inter-chains interactions [Tiwari et al. (2015)]. After 300 °C, there is a gradual weight loss due to the decomposition of the polymer chain [48]. For 1:2 g-C_3N_4-PIn nanohybrid, the

significant thermal stability of TGA curves (Figure 3.9c) in between 200 to 500°C was observed compared to the pure PIn and effective weight loss thereafter. This indicates that surface coating affects the conjugation between g-C_3N_4 and PIn at their interface resulting in better thermal stability.

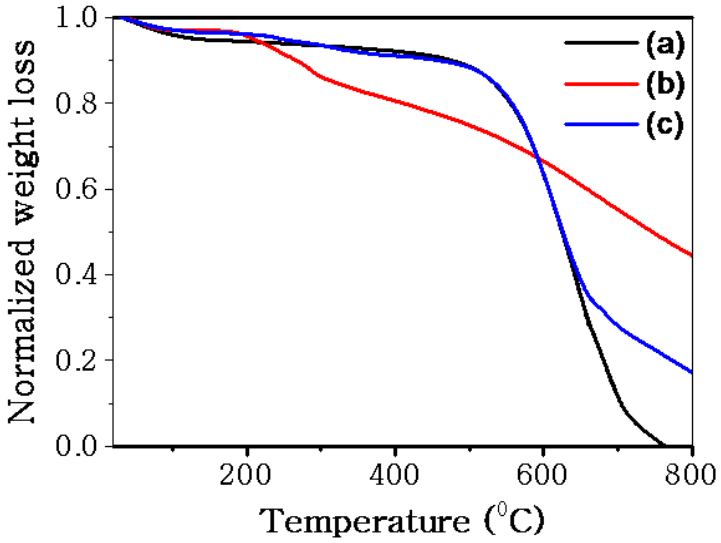

Figure 3.9 TGA curves of (a) bare g-C_3N_4, (b) pure PIn and (c) 1:2 g-C_3N_4-PIn nanohybrid

3.3.4. Electrochemical studies:

In order to explore the electrochemical performance of the synthesized nanohybrids, CV experiments were performed by using the three-electrode setup in 1M H_2SO_4 as an electrolyte. Figure 3.10A shows the combined CVs of g-C_3N_4-PIn nanohybrids along with bare g-C_3N_4, pure PIn, and bare GCE at 50 mVs^{-1} scan rate. The bare g-C_3N_4 electrode exhibits a quasi-rectangular shape with a negligible redox peak, which represents nearly EDLC behavior instead of pure EDLC as carbon-based electrodes [Wu et al. (2017), Jiang et al. (2017)]. This is because of the presence of N heteroatom in the carbon matrix of g-C_3N_4. The area under the CV curve corresponding to the g-C_3N_4 electrode is very small reveals the poor electroactivity. However, after surface

modification by PIn, the electroactivity of the resulting nanomaterials becomes improve. This is because of the conducting nature of PIn which reduces the path resistance of charge transfer over the electrode surface. In comparison with all (Figure 3.10A), the graph reveals that the enclosed area under the CV curve of 1:2 g-C_3N_4-PIn electrode is significantly large compared to the parental materials (bare g-C_3N_4 and pure PIn) alone as well as other nanohybrid electrodes. This indicates, the electrochemical performance is directly related to the amount of PIn. As the PIn amount changed from 1:0.5 g-C_3N_4-PIn to 1:2 g-C_3N_4-PIn is attributed to increments in its electrochemical response, but the further amount of PIn as in 1:5 g-C_3N_4-PIn nanohybrids has reduces the electrochemical response. The CV of pristine PIn showing less area under the curve indicate poor performance because of due to strong interaction between the polymer chain which makes a compact structure and hinders the charge transportation. In this consequence, both less, as well as more amount of PIn, give an adverse effect on its electrochemical performance. This may be attributed to the small amount of polymer that is not sufficient for surface coating of g-C_3N_4 uniformly as in 1:0.5 g-C_3N_4-PIn nanohybrid, while in the case of 1:5 g-C_3N_4-PIn nanohybrid, the polymer dominancy caused a compact structure and change their interfacial arrangements because of a strong interaction between the polymer chains. The higher amount of indole monomer results in a thick layer that can infer the transportation of ions/charge. The surface architecture variations are observed for the same in HRSEM and TEM (Figureb 3.7 and Figure 3.8). This study reveals that the overloading of PIn is useless, and blocking the synergistic effect which is between the PIn with g-C_3N_4 nanosheets. Further, the 1:2 g-C_3N_4-PIn nanohybrid electrode shows

quite distinct redox peaks at around 0.5 V corresponding to the polaronic (doping/dedoping) transitions of different forms of PIn that provide larger pseudocapacitance [Wang et al. (2017)]. Furthermore, the study of the kinetic response of 1:2 g-C_3N_4-PIn nanohybrid electrode was performed by the CV measurements at different scan rates (20, 50, 100, and 150 mVs^{-1}) and shown in Figure 3.10B. We have observed that with increasing scan rate, the shape of CV curves retains even up to very high scan rate of 150 mVs^{-1} along with the continuous increase of peak current and minimal shift of anodic/ cathodic peak positions, indicating good reversibility and the typical feature of pseudocapacitive materials having good rate capability to storage [Chen et al. (2015), Zhou et al. (2015)]. According to Figure 3.10B, we observed the redox peaks with a linear behavior between current and scan rate which indicates the electrode reaction is under diffusion-controlled process [Piriya et al. (2018)].

At the same time, we also observed that, on increasing the concentration of APS during polymerization of indole monomer, the PIn formed in 1:2::indole:APS ratio exhibit better electroactive property than other counterparts (for details *see* Effect of different APS concentration on electrochemical performance Figure 3.13).

Furthermore, GCD measurements were performed for the as-synthesized electrode materials. Figure 3.10C presents the comparative GCD curves of g-C_3N_4-PIn nanohybrids along with bare g-C_3N_4 and pure PIn in the potential range of -0.2 to +1.0 V at a current density of 2 Ag^{-1}. It can be seen that charge and corresponding discharge curves are quite symmetrical, representing good reversibility of electrode materials.

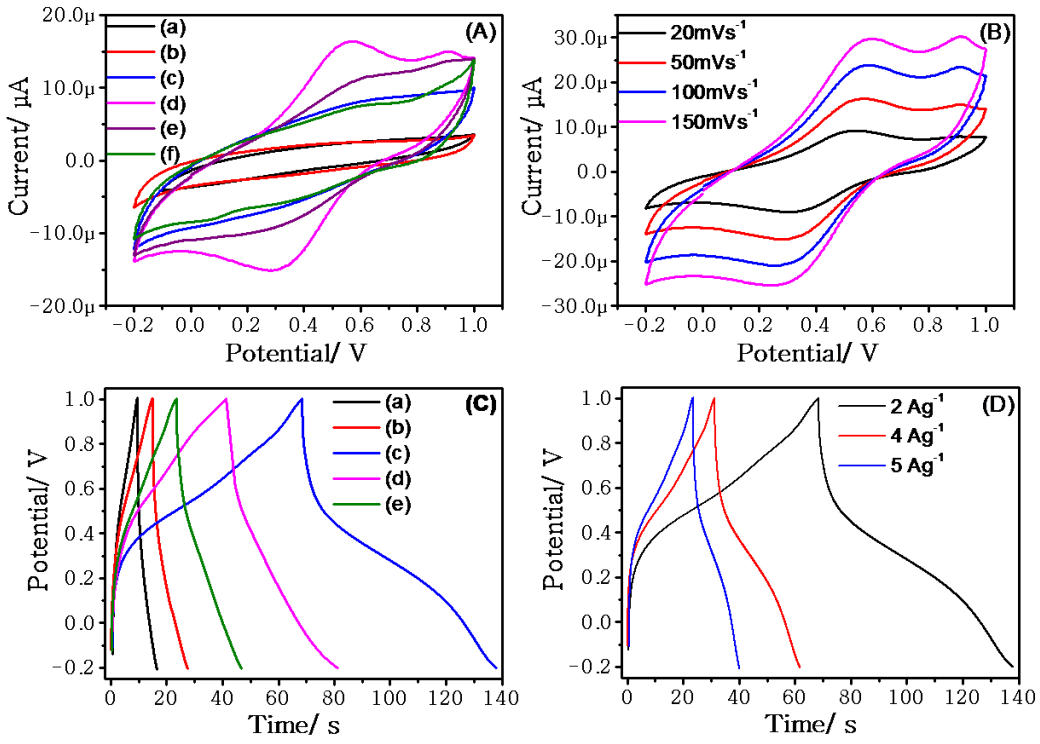

Figure 3.10 (A) Combined CV graph of glassy carbon (a), bare g-C_3N_4 (b), 1:0.5 (c), 1:2 (d), 1:5 (e) g-C_3N_4-PIn nanohybrids and pure PIn (f) electrodes at 50 mVs^{-1} scan rate in 1.0 M H_2SO_4; (B) CV curves of 1:2 g-C_3N_4-PIn nanohybrid electrode in1.0 M H_2SO_4 at various scan rates; (C) combined GCD graph of bare g-C_3N_4 (a), 1:0.5 (b), 1:2 (c), 1:5 (d) g-C_3N_4-PIn nanohybrids and pure PIn (e) electrodes in 1.0 M H_2SO_4 at 2 Ag^{-1} current density; (D) GCD curves of 1:2 g-C_3N_4-PIn nanohybrid electrode in 1.0 M H_2SO_4 at various current density.

The Cs calculations are performed using the following formula:

$$Cs = \Delta t \times I / (\Delta V \times m)$$

Where Δt is the discharge time, I is applied current density, ΔV is voltage range, and m is the mass of the electrode material [Chen et al. (2015), Shayeh et al. (2018)]. The calculated value of Cs for 1:2 g-C_3N_4-PIn is 115.8 Fg^{-1} which is much higher than that of bare g-C_3N_4, pure PIn, and others nanohybrids like 1:0.5 and 1:5 g-C_3N_4-PIn electrodes Cs value as 12.4, 38.7, 21.5, and 66.9 Fg^{-1}, respectively. Such enhancement

of Cs value can be explained due to the synergic interaction between g-C_3N_4 and PIn at an optimized weight ratio for 1:2 g-C_3N_4-PIn nanohybrid. A lower amount of PIn as in 1:0.5 g-C_3N_4-PIn nanohybrid resulted in poor interfacial interaction while the higher amount in 1:5 g-C_3N_4-PIn nanohybrid imparts overdose and consequently loss of synergistic effect between two counterparts. Figure 3.10D shows the GCD curve of 1:2 g-C_3N_4-PIn nanohybrid electrode at a different current density ranging from 2 to 5 Ag^{-1}. From this, the GCD curve has consistency in their shape without any deviation which indicating the good reversibility of electrode materials. The GCD graph illustrates that the time required for the charge-discharge process of the electrode decreases by increasing the current density.

Furthermore, the interfacial charge transfer process between the modified GCE electrode and the electrolyte was studied by the EIS experiment. Figure 3.11 shows Nyquist plots of as-synthesized g-C_3N_4-PIn nanohybrids along with bare g-C_3N_4 and pure PIn within the frequencies range of 10.0 mHz to 10 kHz at their open circuit potential (OCP). The behavior of all the studied materials shows the impedance variations with respect to the frequency. All the studied electrodes show straight-line nature at lower frequencies and attribute to the diffusion behavior of electrolyte via charge transfer in the electrode materials through diffusion-controlled process [Chen et al. (2015)]. Again, the diameter of the semicircle, which reflects the charge transfer resistance (R_{ct}) at the interface, was almost negligible at the high-frequency region and indicates the low charge transfer resistance due to the fast electron transfer [Zhao et al. (2017), Chen et al. (2015), Shayeh et al. (2018)]. The graph clearly shows that for 1:2 g-C_3N_4-PIn nanohybrid electrode, the Nyquist plot inclined more towards the *Z*” axis

with the smallest semicircle radius compared to other tested materials, which signifies lower R_{ct}, smaller diffusion resistance of ions in this nanohybrid, and better capacitive performance [Zhou et al. (2016)]. This may be due to the fluffy arrangement of polymer within the 1:2 g-C_3N_4-PIn nanohybrids, where electrolyte can penetrate inside the polymer bulk due to the fast transportation of surface charge [Dubey et al. (2015)]. However, due to alone PIn has a compact structure because of strong interactions between its chain which appearing as long straight lines in Nyquist plots (Figure 3.10e) that's why electrolyte ions can't penetrate frequently inside the bulk polymer.

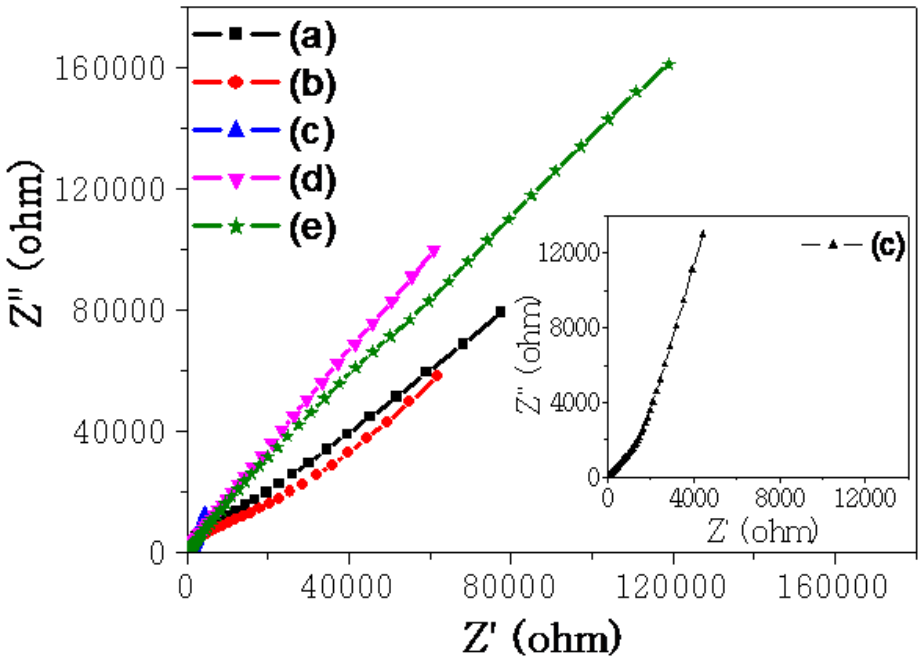

Figure 3.11 Nyquist plots of (a) bare g-C_3N_4, (b) 1:0.5, (c) 1:2, (d) 1:5 g-C_3N_4-PIn nanohybrids and (e) pure PIn electrodes at their OCP (inset shows enlarged view of 1:2 g-C_3N_4-PIn nanohybrid electrode).

When this polymer applied for modification g-C_3N_4 surface with optimal weight ratio (1:2 g-C_3N_4-PIn), the resulting nanohybrids get fluffy and homogeneous open structures. However, when polymer amount crosses the optimal as in 1:5 g-C_3N_4-PIn,

the arrangement becomes compact which hinders the charge transportation. Thus, the charge amassing order of the as investigated electrode materials are bare g-C_3N_4< 1:0.5 g-C_3N_4-PIn < pure PIn< 1:5 g-C_3N_4-PIn< 1:2 g-C_3N_4-PIn nanohybrids, which is consistent with the CV and GCD results.

Further cyclic stability test of optimized 1:2 g-C_3N_4-PIn nanohybrids has performed in the same condition which is depicted that the 1:2 g-C_3N_4-PIn nanohybrid electrode has 95% retention in their performance over the 250 cycles (shown in Figure 3.12). In this, at starting the performance become high as cycle ramping, because of swelling in electrode material which allows to access more charge/ions.

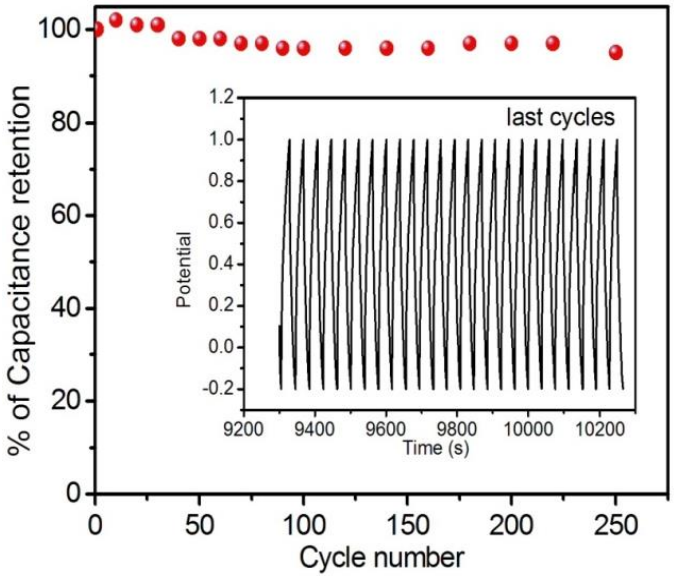

Figure 3.12 Cyclic stability test of 1:2 g-C_3N_4-PIn nanohybrid electrode at $5Ag^{-1}$.

3.3.5 Effect of different APS concentration on electrochemical performance:

Since the polymerization reaction begins with oxidation under various oxidizing agents (APS, $FeCl_3$ etc.), and directly related to the nucleation process. As the APS

concentration goes to high, the nucleation process becomes very fast which leads to the secondary growth and quickly terminates the polymerization reaction that can cause the globular shape to shorten the polymer chain length. In order to analyze the effect of different APS concentrations on electrochemical performance of 1:2 g-C_3N_4-PIn nanohybrids (which is showing better performance), we have prepared three combinations 1:1, 1:2 and 1:4 molar ratio of indole and APS (1:2 g-C_3N_4-PIn ratio fixed for each). The SEM morphology is shows variation in their surface textures. From Figure 3.13, SEM image of (I) corresponding to 1:1::Indole: APS ratio showing in homogeneous surface coating. This is because of at such ratio, insufficient of APS, and results in incomplete polymerization. Further, when the APS ratio increased for 1:2, this is sufficient condition where the indole monomer undergoes to the polymerization process. That gives a homogenous surface coating of g-C_3N_4 (*see* in Figure 3.13II). However, if a high amount of APS used (as in 1:4::Indole: APS), the globular like shape appeared (*see* in Figure 3.13III). This is because, at high concentration of APS, there are lots of nucleation sites may increase the polymerization reaction and terminate this quickly. Due to insufficient time, the length of the polymer becomes distracted into small globular shape. In other words, less amount of APS, polymerization will not complete however at high concentration polymer becomes over oxidized.

The CV curves (Figure 3.13a-c) showed the 1:2 Indole: APS (as in Figure 3.13(b)), a larger integrated area, thus indicating for high electrochemical performance. Also, there are redox peaks corresponding doping/dedoping similar to results as discussed in our main text. The CV of 1:1::Indole: APS shown in Figure 3.13a, is showing a very

small integrated area under the curve, and no visible redox peak which indicates that this ratio is not good. This is because such an amount of APS is not sufficient to complete the polymerization. During this reaction, huge numbers of oligomers are formed. Those wash out under the ethanol washing process. Therefore, in this case, g-C_3N_4 characteristics are reflected. However, the CV curve of a material prepared under a high amount of APS (as in Figure 3.13III 1:4::Indole: APS), show the lowering in their integrated area under the curve. This can be explained as a high concentration of APS, a fast nucleation process that results in a globular shape. These all are showing the normal relation between current and scan rate.

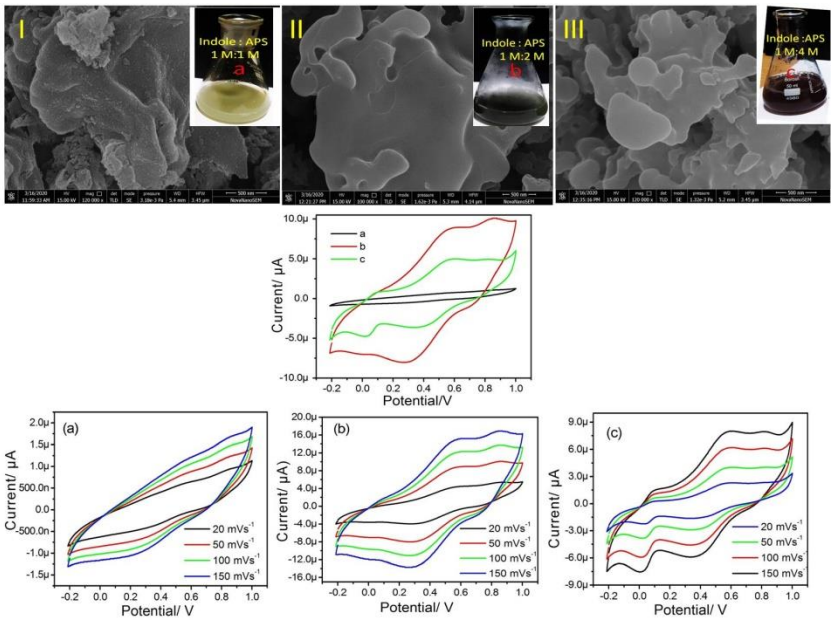

Figure 3.13 SEM image of (I) 1:1, (II) 1:2 and (III) 1:4::Indole : APS ratios, and its CV graph as (a) 1:1, (b) 1:2 and (c) 1:4 respectively. (Note-1:2 g-C_3N_4-PIn ratio used for each)

To further understand the electrode reaction kinetics, CV at the different scan rate in the range of 20−150 mVs^{-1} (as Figure 3.10B and Figure 3.13(a-c)) giving a linear

behavior between current density and scan rate in consequence to diffusion-controlled process occur between electrolyte medium to electrode surface [Piriya et. al. (2018)].

3.4. **Conclusion**

In summary, interfacial engineering between g-C_3N_4 nanoflakes and PIn is performed by a simple one-step *in-situ* chemical polymerization. The existence of PIn over g-C_3N_4 surface is validated by various characterization experiments which reveal that nanohybrids have different molecular arrangements as amounts of PIn used. 1:2 g-C_3N_4-PIn is an optimized composition ratio and exhibits improved electrochemical performance over other studied electrode materials. Effect of different APS concentrations on electrochemical performance also investigated which reveals the 1:2 ratio is optimum for Indole:APS. The estimated Cs value is 115.8 Fg^{-1} at 2 Ag^{-1} current density in 1.0M H_2SO_4. This electrode shows a 95% retention in their performance over 250 cycles. Here, we suggest that g-C_3N_4-PIn nanohybrids may be one of the emerging candidates as a metal-free electrode material for electrochemical applications such as supercapacitor.